Adaptive Mesh Refinement for Micromagnetics Simulations

Carlos J. García-Cervera, and Alexandre M. Roma

***Abstract*— We present a methodology to perform efficiently micromagnetics simulations which combines an unconditionally stable, finite differences scheme with an adaptive mesh refinement technique. Enhanced accuracy is attained by covering locally special regions of the domain with a sequence of nested, progressively finer rectangular grid patches which dynamically follow sharp transitions of the magnetization field (e.g., walls and vortices). To illustrate our approach, we consider a rectangular sample of infinite thickness with strong anisotropy in the out-of-plane direction.**

***Index Terms*— Landau-Lifshitz-Gilbert, Multilevel-multigrid, Finite Differences, Adaptive Mesh Refinement**

I. Introduction

UNDERSTANDING the mechanisms of magnetization reversal in ferromagnetic samples of nanoscale size is of interest in the study of the magnetic recording process, in particular in computer disks and in computer memory cells, such as MRAMs [1], [2].

The relaxation process of the magnetization distribution in a ferromagnetic material is described by the Landau-Lifshitz-Gilbert equation (LLG) equation [3], [4],

$$\mathbf{M}_t = -\gamma \mathbf{M} \times \mathcal{B} - \frac{\gamma\alpha}{M_s} \mathbf{M} \times (\mathbf{M} \times \mathcal{B}), \qquad (1)$$

where $|\mathbf{M}| = M_s$ is the saturation magnetization which, far from the Curie temperature, is usually set to be a constant; the first and second terms are the gyromagnetic and the damping terms, respectively, with γ being the gyromagnetic ratio, and α the dimensionless damping coefficient; $\mathcal{B}$ is the effective field

$$\mathcal{B} = -\frac{1}{M_s} \nabla_{\mathbf{u}} \Phi \left(\frac{\mathbf{M}}{M_s} \right) + \frac{C_{ex}}{M_s^2} \Delta \mathbf{M} + \mu_0 (\mathbf{H}_s + \mathbf{H}_0). \qquad (2)$$

Carlos J. García-Cervera is currently at the Mathematics Department, University of California, Santa Barbara, CA 93106, USA. URL: http://www.math.ucsb.edu/~cgarcia. Email: cgarcia@math.ucsb.edu

Alexandre M. Roma is currently at the Departamento de Matemática Aplicada, Universidade de São Paulo, Instituto de Matemática e Estatística, Caixa Postal 62281, CEP 05311-970, São Paulo - SP, Brasil. URL: http://www.ime.usp.br/~roma. E-mail: roma@ime.usp.br

In (2), $\Phi(\mathbf{u})$ represents the anisotropy energy per unit volume. The parameters C_{ex} and μ_0 are the exchange constant and permeability of vacuum, respectively. $\mathbf{H}_s$ is the stray field, and $\mathbf{H}_0$ is the external field.

Typically, the magnetization profile in a ferromagnetic sample displays large domains where the magnetization is slowly varying. These domains are usually of the order of a few hundreds of nanometers in size, and are separated by magnetic walls, and magnetic vortices. The core size of these sharp transition regions is of the order of a few nanometers. Most experimental studies coincide that the presence of magnetization vortices inside a ferromagnetic sample has a dramatic effect in the magnetization reversal process [5], [6], [7], [8], [9]. In addition, the reversal process occurs as a consequence of domain wall motion. In order to carry out realistic micromagnetics simulations, it is therefore necessary to resolve numerically a broad range of length scales, spanning from the nanometer size magnetic walls and vortices to the macroscopic size of magnetic memories and hard drives. Moreover, the overall accuracy of the numerical simulation depends strongly on how well these local phenomena are resolved [10].

Fully resolved three dimensional simulations that use a uniform grid may result too costly for currently available computer resources. To increase the computational efficiency, and to allow for complex problems to be tackled, reductions in the processing time and in the computer memory consumption are desirable. These reductions can be achieved by adaptively refining the spatial mesh locally around walls and vortices, while resolving magnetic domains with a coarser grid.

In micromagnetics simulations, the adaptivity has usually been achieved by employing adaptive refinement finite element methods [11], [12], [13], or by employing methods based on a moving mesh [14], [15], [16].

Adaptive finite elements started to be applied to several problems in micromagnetics in the nineties. Among those are the simulations of longitudinal thin film media [11], domain structures in soft magnetic thin films [12], and domain wall motion in permanent magnets [13], to name a few. Arbitrarily shaped domains can be handled naturally by finite element discretizations. Due to the

way information is stored and retrieved at nodal points, the mesh adaptivity may impose a relatively heavy computational overhead when compared to the processing time taken by the overall method, especially if remeshing must be performed frequently.

In the moving mesh method, a mapping between a uniform logical mesh and the physical mesh is defined. The physical mesh deforms from one time step to the next in order to accommodate the underlying structure of the solution. The new mapping may be obtained either by an optimization procedure [17], or dynamically, as in [18]. This methodology has been employed in the study of singularity formation in different contexts [19], [18]. In this procedure, the equations on the physical grid are rewritten on the logical grid. This gives rise to a differential equation with non-constant coefficients. In the context of micromagnetics, this may complicate considerably the stray field computation.

Here, we introduce another strategy for adaptive micromagnetics simulations which combines the Gauss-Seidel Projection Method (GSPM) [10], [20] with an adaptive mesh refinement (AMR) technique. The GSPM is an unconditionally stable scheme for micromagnetics simulations whose complexity is comparable to that of solving the linear heat equation with the Backward Euler Method. The AMR technique employed is based on the works of Berger and Collela [21], for solving hyperbolic equations on rectangular grids, and Berger and Rigoutsos [22], for point clustering and mesh generation. Enhanced accuracy is attained by covering certain regions of the domain with a sequence of nested, progressively finer rectangular grid patches which dynamically follow special features of the solution (e.g., sharp property transitions). Since the convergence properties of the GSPM are well understood on rectangular grids, this refinement technique seems to be particularly appealing. Moreover, rectangular grids have a simple user interface and, by separating the integration method from the adaptive strategy, we can use the GSPM on fine and coarse grids without modification.

By combining the GSPM with the AMR, we obtain an unconditionally stable, adaptive method for the simulation of the LLG equation on rectangular domains, with optimal asymptotic complexity. Second-order finite differences for spatial approximations are employed and only the solution of Poisson-type equations with constant coefficients are required. Although we only consider a rectangular sample, arbitrarily shaped domains can be handled efficiently by carefully adding boundary corrections to the exchange and stray fields [23].

For the reasons above, the AMR-GSPM is an attractive alternative approach to both adaptive finite elements and moving mesh methods. We illustrate our approach by finding the steady state of the magnetization in a rectangular sample of infinite thickness, with strong anisotropy in the out-of-plane direction, and for which a large number of complex, transient structures develop.

II. Micromagnetics Simulations

The Landau-Lifshitz-Gilbert equation (1) is solved employing the Gauss-Seidel Projection Method [10], [20]. Only linear systems of the form

$$(I - \Delta t\, \Delta)\, \mathbf{M} = \mathbf{f} \tag{3}$$

must be solved. By carefully introducing the nonlinearity *a posteriori*, an unconditionally stable finite differences method for the LLG equation is obtained, and we may employ time steps on the order of 1 picosecond, even in the presence of thermal agitations [20].

The stray field can be written as $\mathbf{H}_s = -\nabla U$, where U is the magnetostatic potential. U solves the magnetostatic equation

$$\begin{aligned} \Delta U &= \text{div } \mathbf{M}, \quad \mathbf{x} \in V \\ \Delta U &= 0, \quad \mathbf{x} \in \overline{V}^c \\ [U] &= 0, \quad \mathbf{x} \in \partial V \\ \left[\frac{\partial U}{\partial \nu}\right] &= -\mathbf{M} \cdot \nu, \quad \mathbf{x} \in \partial V, \end{aligned} \tag{4}$$

where V is the volume occupied by the sample, and $[\bullet]$ represents the jump at the material/vacuum interface. Equation (4) must be solved in the whole space. This requires the introduction of far field boundary conditions. In order to avoid this, we decompose the potential into two parts: $U = v + w$. The function w satisfies equation

$$\begin{aligned} \Delta w &= \text{div } \mathbf{M}, \quad \mathbf{x} \in V, \\ w &= 0, \quad x \in \partial V, \end{aligned} \tag{5}$$

and it contains the bulk contribution of div $\mathbf{M}$ to the stray field. The function w is extended to be equal to zero outside V.

The boundary contributions are included in v, which satisfies equation

$$\begin{aligned} \Delta v &= 0, \quad \mathbf{x} \in V \cup \overline{V}^c, \\ [v] &= 0, \ \mathbf{x} \in \partial V, \\ \left[\frac{\partial v}{\partial \nu}\right] &= -\mathbf{M} \cdot \nu + \frac{\partial w}{\partial \nu}, \ \mathbf{x} \in \partial V. \end{aligned} \tag{6}$$

The solution to (6) is

$$v(\mathbf{x}) = \int_{\partial V} N(\mathbf{x} - \mathbf{y}) g(\mathbf{y})\, d\sigma(\mathbf{y}), \tag{7}$$

where $g(\mathbf{y}) = -\mathbf{M} \cdot \nu + \frac{\partial w}{\partial \nu}$, and N is the Newtonian potential in free space. Formula (7) can be used to

evaluate v on the boundary of the domain, and therefore v can be determined inside the domain solving equation (6) with Dirichlet boundary data. This approach is similar to the hybrid method introduced by Fredkin and Koehler [24]. Our approach differs in that we use Dirichlet boundary conditions instead of the Neumann boundary conditions considered in [24], which changes the integral representation of the boundary contribution from a double layer potential, to the single layer potential (7). The single layer potential is less singular than the double layer potential, and thus can be handled numerically more easily.

We approximate integral (7) on the boundary of the domain by approximating g using piece-wise polynomial interpolation. The corresponding moments of the Newtonian potential can be evaluated analytically. In two dimensions, the resulting sum can be evaluated in $O(N)$ operations by direct summation, where N is the total number of grid points in the domain, if a uniform grid was used. In three dimensions, however, the evaluation of the boundary values by direct summation is an $O(N^{\frac{4}{3}})$ operation. Solving Poisson's equation with Multigrid [25] is an $O(N)$ operation. Therefore, in two dimensions our procedure has optimal complexity. In three dimensions, the evaluation of the boundary values by direct summation dominates the CPU time. The computational time can be further reduced using a fast summation technique [26], [27]. Results in this direction will be presented elsewhere.

III. Adaptive Mesh Refinement

In our approach, the ferromagnetic sample is covered by *composite grids*, that is, by block-structured grids, defined as a hierarchical sequence of nested, progressively finer levels. Each level is formed by a set of disjoint rectangular grids and the refinement ratio between a level and the next finer level is two. The magnetization is defined at the center of the computational cells. Ghost cells are employed around each grid, for all levels, and underneath fine grid patches to formally prevent the finite differences operators from being redefined at grid borders and at interior regions which are covered by finer levels. We use second- or third-order accuracy interpolation schemes to provide values at these cells. The description of the composite grids is given in [21] in greater detail. In Fig. 1, we show an interface between two successive refinement levels, and the location of coarse and fine variables.

The use of an unconditionally stable time stepping procedure such as the GSPM allows us to evolve the solution on all grids, and in all levels, with the same time step. The complexity of the GSPM is comparable to that of solving a linear heat equation using Backward Euler. Equations (3), (5), and (6) are solved using a multilevel-multigrid method [28], [29].

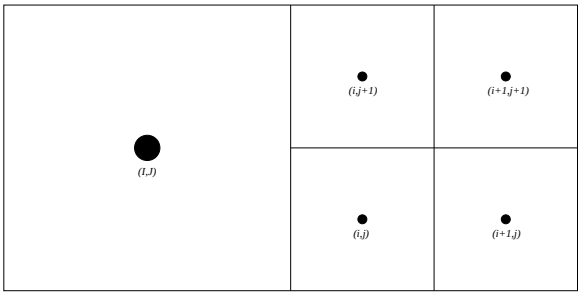

Fig. 1. Ghost cells near the interface.

A. Composite Grid Generation and Remeshing

Composite grid generation depends on the *flagging step*, that is, determining first the cells whose collection gives the region where refinement is to be applied. We mark for refinement the cells at which the absolute value of the in-plane divergence of the magnetization field is at least 10% of its global maximum, that is, if

$$|\nabla \cdot \big(M_1(\mathbf{x}_{ij}), M_2(\mathbf{x}_{ij}), 0\big)| \geq 0.10 \max_{rs}\{\, |\nabla \cdot \big(M_1(\mathbf{x}_{rs}), M_2(\mathbf{x}_{rs}), 0\big)| \,\}. \quad (8)$$

Also, it is convenient to mark for refinement a layer of cells close to the boundary of the domain. This way, we are able to compute the boundary integral given by (7) with the accuracy of the finest level.

Other criteria that can be employed for marking cells for refinement, either simultaneously or separately, are the norm of the gradient of the angle formed by the two in-plane components, and the norm of the rotational of the field, $||\nabla \times \mathbf{M}||$.

Once the collection of flagged cells is obtained, grids in each level are generated by applying the algorithm for point clustering proposed by Berger and Rigoutsos [22]. We require that, at least, from 70% to 85% of the cells in each grid patch were flagged (grid *efficiency*). The rest of the cells are included so the grid patch is rectangular.

Remeshing is performed in two situations: 1) whenever high in-plane divergence values escape from the region covered by the finest level, and 2) at every certain number of fixed time steps (e.g., at every 50 time steps) in order to refresh the composite grid; otherwise, composite grids generated with finest levels covering a large portion of the domain would tend to stay permanently in use, and the integration would become inefficient.

IV. Results

To illustrate the proposed methodology, we consider a rectangular cylinder of infinite thickness parallel to the OZ-axis, with strong anisotropy in the out-of-plane direction. The Landau-Lifshitz energy per unit length becomes

$$F[\mathbf{M}] = \frac{K_u}{2M_s^2}\int_V M_3^2\,d\mathbf{x} + \frac{C_{ex}}{2M_s^2}\int_V |\nabla \mathbf{M}|^2\,d\mathbf{x} - \frac{\mu_0}{2}\int_V (\mathbf{H}_s + 2\mathbf{H}_0)\cdot\mathbf{M}\,d\mathbf{x}, \quad (9)$$

where K_u is the anisotropy constant, and V is a rectangle in the XY-plane. The effective field reduces to

$$\mathcal{B} = -\frac{K_u}{M_s^2}M_3\mathbf{e}_3 + \frac{C_{ex}}{M_s^2}\Delta\mathbf{M} + \mu_0\left(\mathbf{H}_s + \mathbf{H}_0\right), \quad (10)$$

where $\mathbf{e}_3 = (0,0,1)$. The stray field is computed solving equation (4) in two dimensions.

The rectangular domain has dimensions $1\mu m \times 250\,nm$. We choose the exchange constant and saturation magnetization to mimic Permalloy ($C_{ex} = 1.3\times10^{-11}J/m$, $M_s = 8\times10^5 A/m$). The anisotropy constant is chosen such that $K_u = \mu_0 M_s^2$, in order to impose a high penalty on the out-of-plane component of the magnetization. The damping parameter was set to $\alpha = 10^{-2}$.

Our motivation to study this problem is twofold. On the one hand, the energy (9) resembles the energy of a thin ferromagnetic film, where the shape anisotropy penalizes out-of-plane excursions of the magnetization, and the leading term in the in-plane components of the stray field is given by a logarithmic convolution kernel [30], [31], [32]. On the other hand, the geometric setting and the parameters considered here allow us to reduce the problem to a two dimensional computation, which simplifies the evaluation of the stray field. Despite this reduction, the minimizers of energy (9) show complex domain structures, with magnetic walls and vortices, making this an ideal test problem for the numerical method presented here.

The domain is discretized employing four levels. Level 1 (the base level) is a uniform grid given by 128×32 cells, on top of which we add three refinement levels. A uniform grid would require 1024×256 cells (that is, 262,144 cells) to have its resolution equivalent to the finest level.

The solution is evolved in time until no visible difference in the magnetization field between successive time steps is noticeable. The final time is 1.5 nanoseconds, reached in 1,500 time steps. At steady state, the magnetization distribution develops the diamond domain structure depicted in Fig. 2. A sketch of this structure is presented in Fig. 3. The arrows show the direction of the in-plane components of the magnetization. Lengths are measured in units of $L = 1\mu m$.

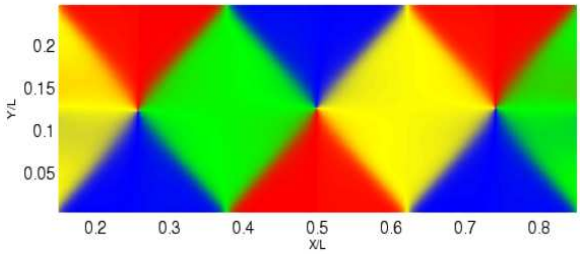

Fig. 2. Diamond domain structure. We present a (color) plot of the angle that the in-plane components of the magnetization form with the OX-axis.

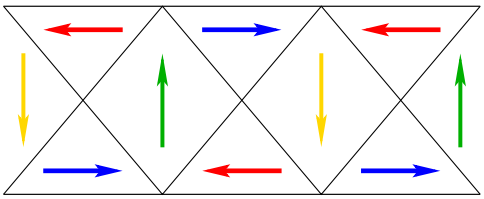

Fig. 3. Sketch of the diamond domain structure. The arrows indicate the direction of the in-plane components of the magnetization.

Employing the divergence of the in-plane components (see Section III-A), and the distance to the boundary of the domain as the flagging criteria, 118 composite grids are generated in the 1,500 time steps. The number of cells in the composite grids, summing over all the levels, ranged from about 51×10^3 to about 213×10^3, the finest level covering from about 11% to about 53% of the domain. In average, the finest level covered only 25% of the domain (6% standard deviation).

Typical grid patches and the corresponding grid cells employed close to the steady state solution are shown in Fig. (4) and (5), respectively. Only the region near one of the vortices is plotted. The composite grid dynamically adapts itself to the underlying structure of the magnetization and concentrates grid points on the domain walls, vortices, and on the boundary of the domain.

To illustrate how the grid patches adapt to the underlying structure of the magnetization, we present different stages in the evolution of the magnetization in Fig. (6) and Fig. (7). Both the magnetization and the corresponding grid patches are plotted. The large number of small structures that arise during the time evolution makes this a good test problem for the procedure presented here.

In Fig. 8, we show the third component of the magnetization at steady state, computed using 128×32 cells. This corresponds to the coarse grid used in Level 1. The exchange length is $l_{ex} = \sqrt{C_{ex}/(\mu_0 M_s^2)} \approx 4\,nm$, and

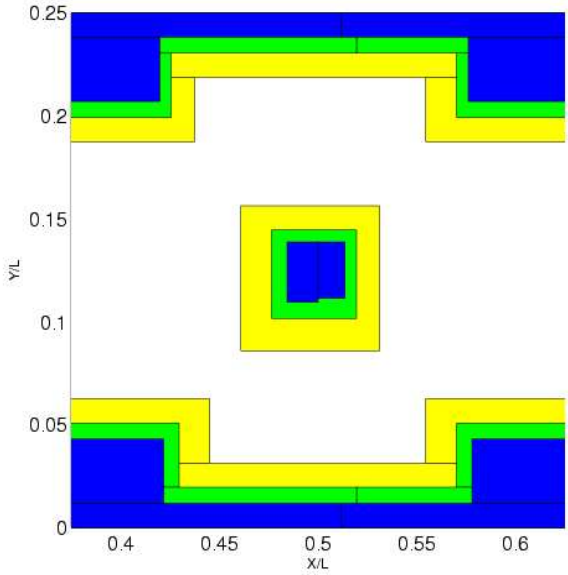

Fig. 4. Grid patches near a vortex and in a neighborhood of the north and south domain boundaries.

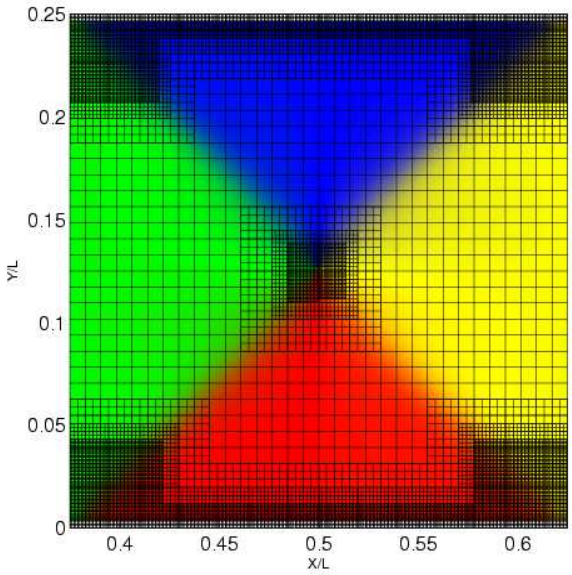

Fig. 5. Grid cells near the vortex shown in Fig. 4.

therefore vortices cannot be resolved with such a coarse grid. This can produce erroneous results, as shown in [10], [33]. For the parameters used in this example, at least 512×128 cells are necessary to resolve the core of the vortex. In Fig. 9, we plot the out-of-plane component of the magnetization computed on the composite grid. The resolution of the composite grid, in a vicinity of the vortex, is equivalent to that of a 1024×256 uniform grid.

To perform the visualization of any function defined on a composite grid, we first interpolate its values to a series of progressively finer uniform grids whose mesh widths range from the mesh width of the base level to the mesh width of the finest level. Remembering that

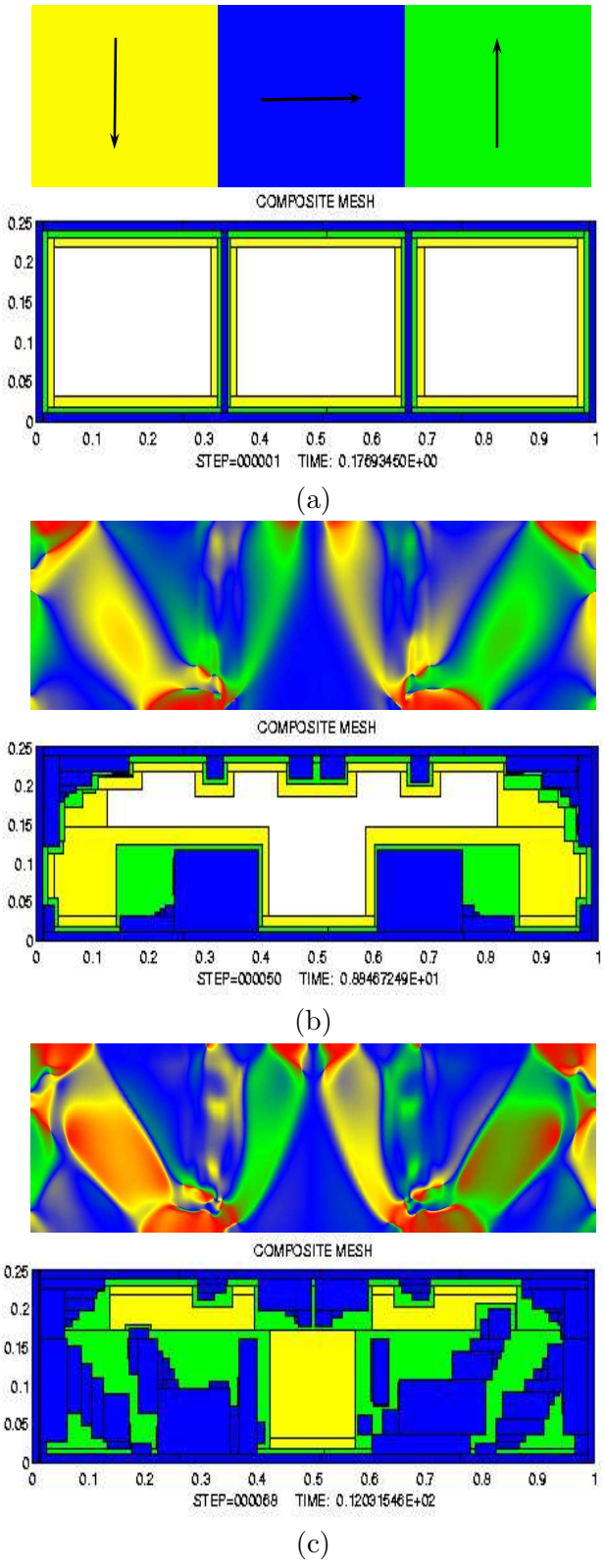

Fig. 6. Evolution of the magnetization towards the diamond structure, with the corresponding grid patches. Darker areas (blue) indicate finer grid patches, while lighter areas (yellow) indicate coarser grid patches. Time is measured in precession time units ($T = (\gamma \mu_0 M_s)^{-1}$). (a) Initial condition. Grid points accumulate at the interface and the domain boundary. The arrows indicate the direction of the magnetization. (b) As finer structures develop, the grid adapts dynamically. (c) Additional patches are added wherever necessary.

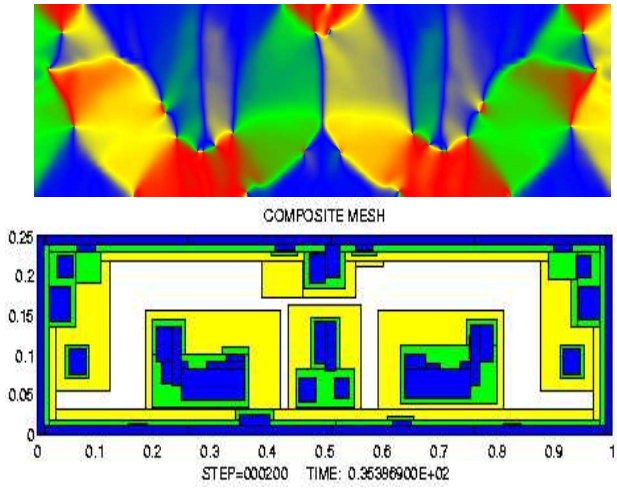

(a)

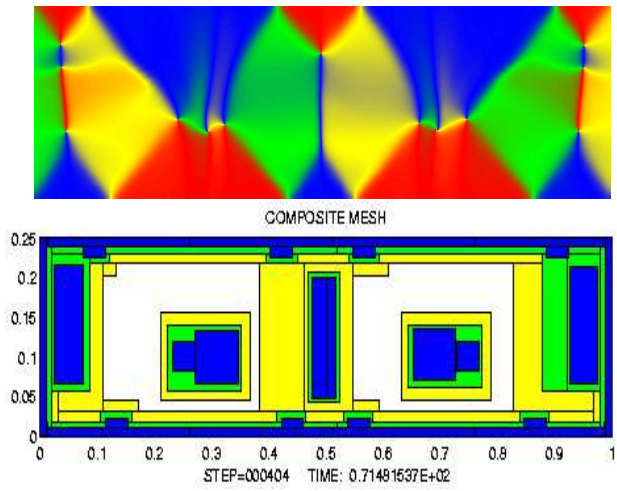

(b)

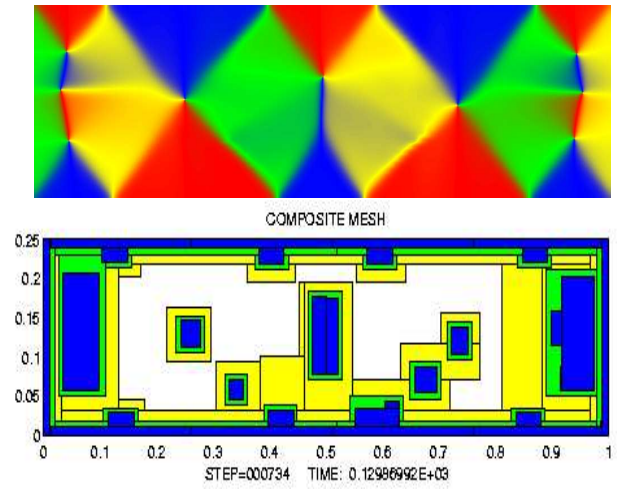

(c)

Fig. 7. (Continuation of Fig. (6)) (a) As the fine structures disappear, fine grid patches are replaced by coarser ones. (b) and (c) The diamond structure is almost formed, and the grid patch distribution becomes more stable.

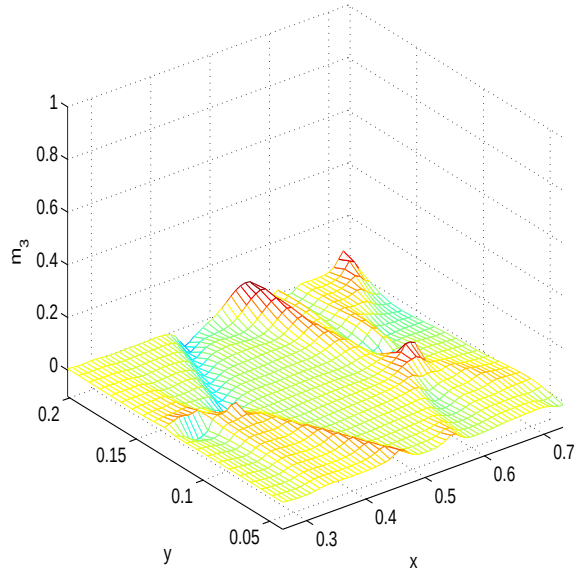

Fig. 8. Out-of-plane component of the magnetization at steady state, computed with a uniform grid, with 128×32 grid points. The vortices cannot be resolved in such a coarse grid.

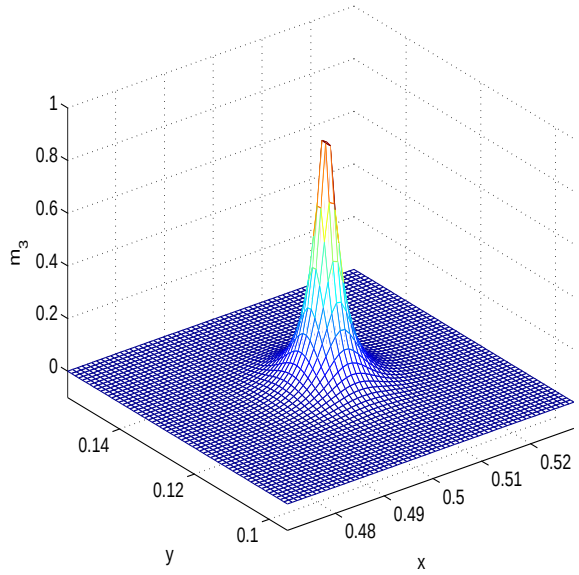

Fig. 9. Out-of-plane component of the magnetization at steady state, on the adaptive grid. The grid around the vortex is equivalent to a uniform grid of 1024×256 grid points. The vortex is fully resolved.

level 1, the base level, is given by a uniform grid, we

1) Interpolate values from the uniform grid with mesh width Δx_k to a uniform grid with mesh width $\Delta x_{k+1} = 0.5\,\Delta x_k$;
2) *Overwrite* the interpolated values with the computed function values coming from level $k+1$ of the composite grid.

We execute this loop for all the levels from 1 to finest level-1.

For the number of levels considered in this example, the steady state solution is obtained on the composite

grid spending less than 65% of the time needed for the equivalent 1024×256 uniform grid, solving in average for about 60% fewer unknowns. For this example, remeshing represents less than 1% of the total processing time.

V. Conclusions

We have presented a finite differences methodology to perform micromagnetics simulations employing adaptive mesh refinement. The spatial grid dynamically adapts itself according to both the size of the divergence of the in-plane components of the magnetization, and the distance from the computational cell to the boundary of the domain.

An unconditionally stable time stepping procedure is employed, allowing for the same time step to be taken for all the grids in all the refinement levels. In particular, we can use large time steps for micromagnetics simulations, and a reduced number of grid points, depending only on the intricate structure of the magnetization.

The Poisson and Helmholtz-type equations are solved using a multilevel-multigrid method, which has asymptotically optimal complexity. The numerical results indicate that greater efficiency in both the processing time and in the memory consumption can be achieved, compared to results obtained with a uniform grid of the same accuracy. Also, remeshing imposes a negligible computational overhead.

Ferromagnetic layers are an integral part of larger structures, such as hard drives, and magnetic memories (MRAMs). An adaptive procedure like the one described here can find applications not only in the study of large ferromagnetic samples, with a variety of small scales, but also in the study of macroscopic devices, such as the ones mentioned before. Although this goal has not been achieved yet, we believe this is a good step in that direction.

As future research, the methodology introduced in this article can be combined with a fast summation technique on adaptive grids to compute the stray field, relaxing therefore the requirement of flagging the cells close to the boundary of the domain for refinement. Also, to deal with arbitrarily shaped domains, boundary corrections can be added to the exchange and stray fields. Results in these directions are natural extensions of this adaptive methodology and will be presented elsewhere.

VI. Acknowledgment

The computations presented in this paper were carried out on a Sun Sparc and a Beowulf cluster purchased by the Mathematics department at UCSB with funds provided by an NSF SCREMS grant DMS-0112388. The authors would like to thank Nathan (Fuzzy) Rogers for his assistance with the computational facilities at the Mathematics Department at UCSB. The work of C.J. García-Cervera was funded by NSF grant DMS-0505738.

References

[1] J. Daughton, "Magnetoresistive memory technology," *Thin Solid Films*, vol. 216, pp. 162–168, 1992.

[2] G. Prinz, "Magnetoelectronics," *Science*, vol. 282, p. 1660, 1998.

[3] W. B. Jr., *Micromagnetics*, ser. Interscience Tracts on Physics and Astronomy. New York - London: Interscience Publishers (John Wiley and Sons), 1963.

[4] L. Landau and E. Lifshitz, "On the theory of the dispersion of magnetic permeability in ferromagnetic bodies," *Physikalische Zeitschrift der Sowjetunion*, vol. 8, pp. 153–169, 1935.

[5] A. Popkov, L. Savchenko, N. Vorotnikova, S. Tehrani, and J. Shi, "Edge pinning effect in single- and three-layer patterns," *Applied Physics Letters*, vol. 77, no. 2, pp. 277–279, 2000.

[6] J. Shi and S. Tehrani, "Edge pinned states in patterned submicron NiFeCo structures," *Applied Physics Letters*, vol. 77, no. 11, pp. 1692–1694, 2000.

[7] J. Shi, S. Tehrani, and M. Scheinfein, "Geometry dependence of magnetization vortices in patterned submicron NiFe elements," *Applied Physics Letters*, vol. 76, pp. 2588–2590, 2000.

[8] J. Shi, T. Zhu, M. Durlam, E. Chen, S. Tehrani, Y. Zheng, and J.-G. Zhu, "End domain states and magnetization reversal in submicron magnetic structures," *IEEE Transactions on Magnetics*, vol. 34, pp. 997–999, 1998.

[9] J. Shi, T. Zhu, S. Tehrani, Y. Zheng, and J.-G. Zhu, "Magnetization vortices and anomalous switching in patterned NiFeCo submicron arrays," *Applied Physics Letters*, vol. 74, pp. 2525–2527, 1999.

[10] X.-P. Wang, C. J. García-Cervera, and W. E, "A Gauss-Seidel Projection Method for the Landau-Lifshitz equation," *J. Comp. Phys.*, vol. 171, pp. 357–372, 2001.

[11] K. Tako, T. Schrefl, M. Wongsam, and R. Chantrell, "Finite element micromagnetic simulation with adaptive mesh refinement," *J. Appl. Phys.*, vol. 81, pp. 4082–4083, 1997.

[12] R. Hertel and H. Kronmüller, "Adaptive finite element techniques in three-dimensional micromagnetic modeling," *IEEE Trans. Magn.*, vol. 34, pp. 3922–3930, 1998.

[13] W. Scholz, H. Foster, D. Suess, T. Schrefl, and J. Fidler, "Micromagnetic simulation of domain wall pinning and domain wall motion," *Comput. Mater. Sci.*, vol. 25, pp. 540–546, 2002.

[14] W. Huang and D. Sloan, "A simple adaptive grid method in two dimensions," *SIAM J. Sci. Comput.*, vol. 15, p. 776, 1994.

[15] S. Li and L. Petzold, "Moving mesh methods with upwinding schemes for time dependent pdes," *J. Comput. Phys.*, vol. 131, pp. 368–377, 1997.

[16] W. Huang and R. Russell, "Moving mesh strategy based on a gradient flow equation for two-dimensional problems," *SIAM J. Sci. Comput.*, vol. 20, pp. 998–1015, 1999.

[17] W. Ren and X. Wang, "An iterative grid redistribution method for singular problems in multiple dimensions," *J. Comput. Phys.*, vol. 159, pp. 246–273, 2000.

[18] H. Ceniceros and T. Hou, "Anefficient dynamically adaptive mesh for potentially singular solutions," *J. Comput. Phys.*, vol. 172, pp. 609–639, 2000.

[19] C. Budd, W. Huang, and R. Russell, "Moving mesh methods for problems with blow-up," *SIAM J. Sci. Comput.*, vol. 17, pp. 305–327, 1996.

[20] C. J. García-Cervera and W. E, "Improved Gauss-Seidel Projection Method for Micromagnetics Simulations," *IEEE Trans. Mag.*, vol. 39, no. 3, pp. 1766–1770, 2003.
[21] M. J. Berger and P. Colella, "Local adaptive mesh refinement for shock hydrodynamics," *J. Comp. Phys.*, vol. 82, pp. 64–84, 1989.
[22] M. J. Berger and I. Rigoutsos, "An algorithm for point clustering and grid generation," *IEEE Transactions on Systems, Man, and Cybernetics*, vol. 21, no. 5, pp. 1278–1286, September-October 1991.
[23] C. J. García-Cervera, Z. Gimbutas, and W. E, "Accurate numerical methods for micromagnetics simulations with general geometries," *J. Comp. Phys.*, vol. 184, no. 1, pp. 37–52, 2003.
[24] D. Fredkin and T. Koehler, "Hybrid method for computing demagnetizing fields," *IEEE Transactions on Magnetics*, vol. 26, no. 2, pp. 415–417, 1990.
[25] Briggs, W.L., *A Multigrid Tutorial*. SIAM – Society for Industrial and Applied Mathematics, 1987, third Edition.
[26] L. Greengard and V. Rokhlin, "A fast algorithm for particle simulations," *Journal of Computational Physics*, vol. 73, pp. 325–348, 1987.
[27] J. Blue and M. Scheinfein, "Using multipoles decreases computation time for magnetic self-energy," *IEEE Trans. Magn.*, vol. 27, pp. 4778–4780, 1991.
[28] M. L. Minion, "A projection method on locally refined grids," *J. Comp. Phys.*, vol. 127, no. 1, pp. 158–178, 1996.
[29] A. M. Roma, C. S. Peskin and M. J. Berger, "An adaptive version of the immersed boundary method," *J. Comp. Phys.*, vol. 153, pp. 509–534, 1999.
[30] C. J. García-Cervera, "Magnetic domains and magnetic domain walls," Ph.D. dissertation, Courant Institute of Mathematical Sciences, New York University, 1999.
[31] C. J. García-Cervera and W. E, "Effective dynamics in thin ferromagnetic films," *J. Appl. Phys.*, vol. 90, no. 1, pp. 370–374, 2000.
[32] C. J. García-Cervera, "One-dimensional magnetic domain walls," *Euro. Jnl. Appl. Math.*, vol. 15, pp. 451–486, 2004.
[33] K. Kirk, M. Scheinfein, J. Chapman, S. McVitie, M. Gillies, B. Ward, and J. Tennant, "Role of vortices in magnetization reversal of rectangular NiFe elements," *J. Phys. D: Appl. Phys.*, vol. 34, pp. 160–166, 2001.